Supporting Information for:

Microstructure vs. Flaw:

Mechanisms of Failure and Strength in Nanostructures

X. Wendy Gu[†], *Zhaoxuan Wu*[°], *Yong-Wei Zhang*[°], *David J. Srolovitz*[+], *Julia R. Greer*[‡]*

[†]Division of Chemistry and Chemical Engineering &

[‡]Division of Engineering and Applied Science, California Institute of Technology,

1200 E. California Blvd., Pasadena, CA 91125, United States

[°]Institute of High Performance Computing, 1 Fusionopolis Way,

#16-16 Connexis, Singapore 138632

[+]Departments of Materials Science and Engineering & Mechanical Engineering and Applied Mechanics, University of Pennsylvania, Philadelphia, PA 19104, United States

Modeling of Notch Geometry

Electroplated nc-Pt nanocylinders were produced with surface notches of several sizes and shapes. Circumferential length, b, and notch height, h, are used to describe the notch geometry and can be measured via scanning electron microscopy (SEM) imaging (Fig. S1). These dimensions can be related to notch depth, a, and notch tip radius, r. a and r are important quantities for determining stress concentrations, but are not easily (or accurately) determined through SEM observations because of limits on imaging resolution and imaging angle.

Observations from SEM allowed the experimental notch geometries to be classified into two types (both with rounded tips): (A) a straight notch that extends across the width of the cylinder (Fig. S1c) and (B) a partial circumferential notch (Fig. S1b). These idealized notch geometries were used in molecular dynamics (MD) simulation and finite element modeling (FEM) in order to compare computer computations with experiment.

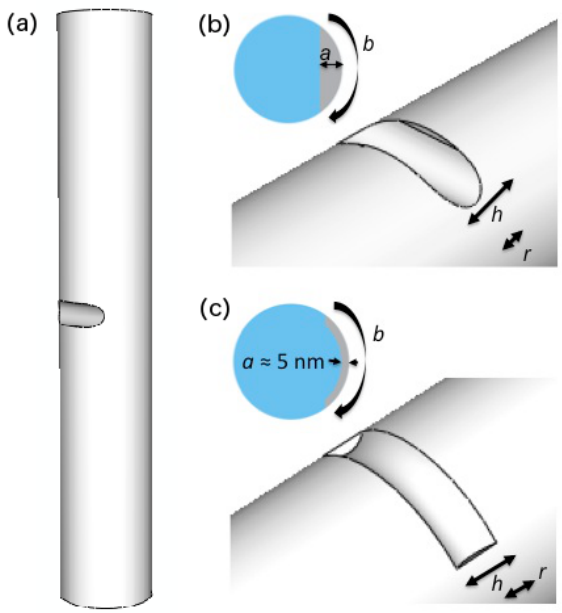

Supplementary Figure S1. (a) Schematic of a cylinder with a rounded notch in the sidewall similar to those in electroplated nc-Pt samples. The experimental notches can be classified as (b) straight notch with a rounded tip that crosses the width of the cylinder (geometry A) and (c) a partial circumferential notch with a rounded tip (geometry B). Notches of both geometries are characterized using circumferential length b, crack height h, and notch radius r, where r is assumed to be equal to $h/2$. Notch depth, a, depends on b in geometry A, and is ~5 nm in geometry B based on SEM observations.

Finite Element Modeling of Notched Cylinders

Finite element modeling (FEM) was performed using ABAQUS/CAE software package in order to calculate the stress concentration at the notch on a cylinder. The sample was modeled as a linear elastic, isotropic, homogenous three-dimensional cylinder with the materials properties of platinum (E = 172 GPa, υ = 0.4) (Fig. S3).

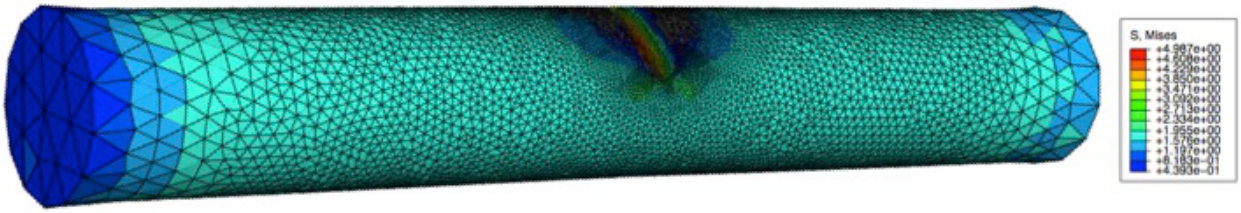

Supplementary Figure S2. Simulated finite element nanocylinder with a notch on the side wall.

Eleven of the twelve experimental samples were modeled using ABAQUS, with notch dimensions consistent with SEM measurements (notch dimensions were not available for the remaining sample). FEM notches were modeled as geometry A, straight notch, or geometry B, partial circumferential notch (Fig. S3).

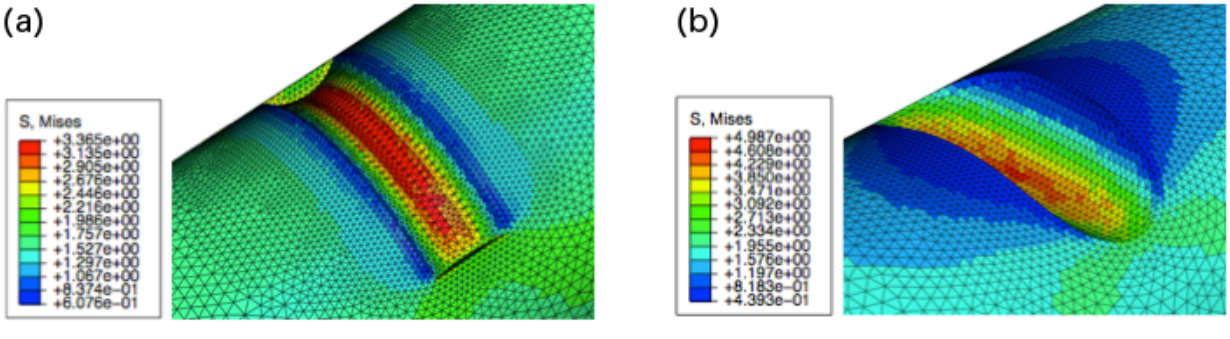

Supplementary Figure S3. Stress contours at the notch for FEM simulated nc-Pt nanocylinders with A) a partial circumferential notch (geometry A) and (B) a straight notch (geometry B).

The FEM sample was statically loaded, with a surface traction applied to one cylindrical base of the cylinder such that the sample was pulled in tension in the z-direction. The sample was fixed in the plane of this cylinder face (to model the constraint imposed by the tension grip). The other cylindrical base was fixed in all three dimensions to model a nc-Pt sample fixed to the substrate. A mesh with 192023 to 463638 tetragonal elements was generated, with the majority of elements concentrated at the notch. The mesh was refined such that the stress values converged to within 7%.

The von Mises stress was calculated at the notch because of the multiaxial stress state present at this location, and used to find the stress concentration at the notch. The stress concentration at the notch for each sample was plotted against ultimate tensile strength (UTS) in Figure S4. Figure S4 shows that samples that broke at the notch had higher stress concentrations at the notch than samples that broke away from the notch for all but one sample, and the distribution in UTS for these two types of failure.

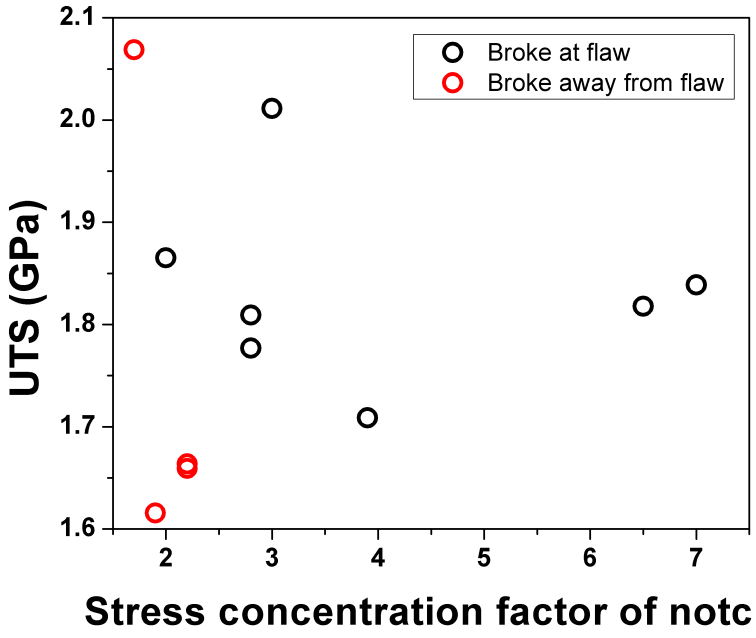

Supplementary Figure S4. Experimentally measured ultimate tensile stress (UTS) versus stress concentration factor for each flaw geometry. Fracture occurs away from the flaw only at relatively small stress concentrations.

Fracture Surface Morphology

After performing tensile tests to fracture, one portion of the tested nanocylinder remains attached to the substrate. The fracture surface was examined by imaging the fractured nanocylinder with scanning electron microscopy. Figure S5 shows a typical fracture surface; the scale of the features on the fracture surface are similar to that of the grains.

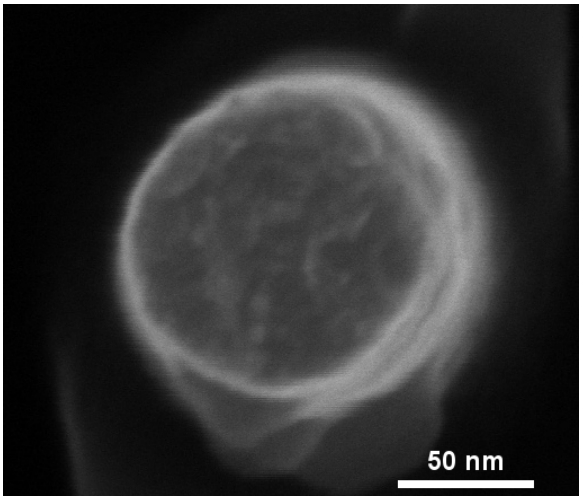

Supplementary Figure S5. SEM image of a typical nanocylinder fracture surface.

Crack Formation at Internal Grain Boundary

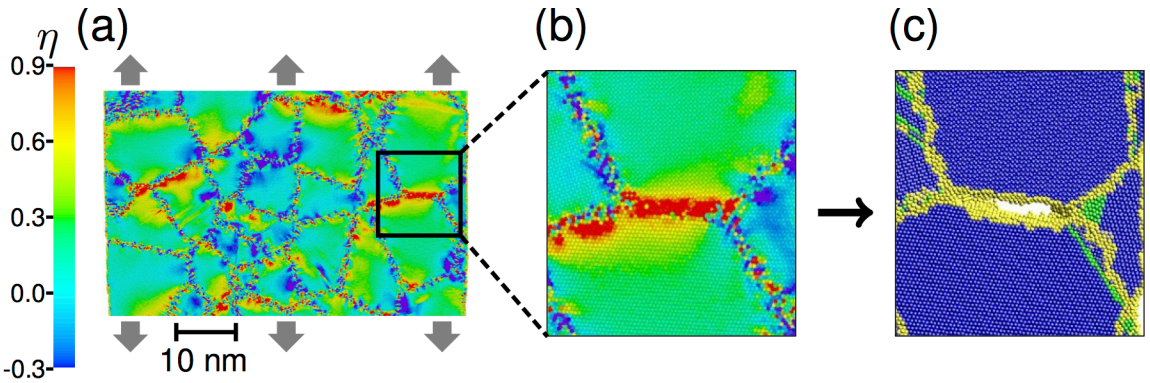

Supplementary Figure S6: (a-b) Cross-sectional view indicating the stress triaxiality η at an applied tensile strain of 6% and (c) subsequent intergranular fracture at an internal grain boundary in a Ni polycrystalline pillar (see Ref. (1) for details). This shows that internal grain boundaries can open in regions of large triaxiality leading to the nucleation of cracks of lengths approximately equal to the length of grain facets.

Molecular Dynamics Movies

Supplementary Movie S1-S5. The deformation, fracture process and stress-strain curves of notch-free nanocylinder (S1) and nanocylinders with different notch geometries (S2-S5) in this study. In each movie, a slice at the middle section of the nanocylinder is shown to reveal the internal fracture process.

Supplementary Movie S6-S8. The evolution of atomistic stress (σ_{yy}) at the middle section of three nanocylinders with different notch geometries. These movies demonstrate dislocation and grain boundary plasticity can effectively blunt notch roots and reduce stress concentrations.

in-situ SEM Movies

Supplementary Movie S9. in-situ SEM video of tension test on nano-cylinder with external flaw which breaks at the flaw.

Supplementary Movie S10. in-situ SEM video of tension test on nano-cylinder with external flaw which breaks away from the flaw.

References

1. Wu ZX, Zhang YW, Jhon MH, & Srolovitz DJ (2013) *Acta Mater.* In Press.